Solid State Communications 371 (2023) 115287

Contents lists available at ScienceDirect

Solid State Communications

journal homepage: www.elsevier.com/locate/ssc

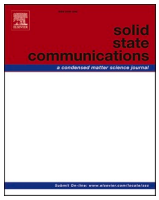

Investigation of phase fraction in α-Fe_2Si_5, ε-FeSi, and β-$FeSi_2$ thermoelectric materials doped with Co and Ni

Sopheap Sam, Kosuke Yamazaki, Hiroshi Nakatsugawa *

Yokohama National University, Yokohama, 240-8501, Japan

ARTICLE INFO

Communicated by: T. Kimura

Keywords:
Iron silicide
Phase fraction
β-$FeSi_2$
ε-FeSi and α-Fe_2Si_5

ABSTRACT

We investigate the phase fraction in Co and Ni-doped β-$FeSi_2$. For the β-$Fe_{1-x}Co_xSi_2$, the formation of the α-phase is more dominant than the ε-phase. In contrast, for the β-$Fe_{1-y}Ni_ySi_2$, the increase in the ε-phase is more dominant than the α-phase. This result indicates the phase transition in β-$FeSi_2$ is dependent on the amount and type of dopant. This study offers a solution to evaluate the phase fraction of Co and Ni-doped β-$FeSi_2$. Therefore, we could identify the range of optimum dopant concentration to prepare Co and Ni-doped β-$FeSi_2$ for thermoelectric application with a preferable phase.

1. Introduction

Iron silicide is an abundant and eco-friendly compound having three types of crystal structures namely tetragonal α-phase (α-Fe_2Si_5 with *P4/mmm* space group) [1], cubic ε-phase (ε-FeSi with $P2_13$ space group) [2], and orthorhombic β-phase (β-$FeSi_2$ with *Cmce* space group) [3]. It should be noted that α and ε-phases are metal and not suitable for thermoelectric (TE) application because of the small Seebeck coefficient ($S = -\Delta V/\Delta T$, where ΔV is the voltage and ΔT is the temperature difference across the material). Among these three phases, semiconducting β-$FeSi_2$ with a small band gap ($Eg \sim 0.7$eV) has been classified as a potential candidate in TE applications due to strong oxidation resistance and good thermal stability [4–6]. The performance of TE material is theoretically defined by the dimensionless figure of merits ($ZT = S^2T\rho^{-1}\kappa^{-1}$, where S is the Seebeck coefficient, T is temperature, ρ is the electrical resistivity, and κ is the thermal conductivity). The term $S^2\rho^{-1}$ is usually known as the power factor (*PF*). Due to low carrier density (n_H) and narrow band gap, the bipolar effect occurs in the pure β-$FeSi_2$ system, resulting in the deterioration of the $|S|$, especially at high temperatures [7]. In addition, the electrical resistivity of non-doped β-$FeSi_2$ is also high because of low n_H [8,9]. Consequently, the ZT value of pristine β-$FeSi_2$ is low ($ZT = 2 \times 10^{-4}$ at 100 K) [10] and this limits its application in thermoelectricity. To solve this issue, researchers have been trying to alloy pure β-$FeSi_2$ with the elements having more valence electrons to either Fe or Si sites for increasing the n_H. However, by adding the dopants, the metallic phases are formed, making the reduction in $|S|$. The analysis of impurity phases was based on the SEM image and XRD patterns [11–17], whereas the quantitative analysis of phases' occupation with Co and Ni dependence in the β-$FeSi_2$ has not been reported. The quantitative analysis of phase fraction is important for designing a good β-$FeSi_2$ for TE application because the phase transition of this material is very sensitive to the dopants.

In this work, we quantitatively report the analysis of the phase fraction of Co-doped β-$Fe_{1-x}Co_xSi_2$ ($0 \le x \le 0.10$) and Ni-doped β-$Fe_{1-y}Ni_ySi_2$ ($0 \le y \le 0.03$) prepared by direct arc melting and heat treatment process. We choose $x \le 0.10$ and $y \le 0.03$ because the optimum condition of Co and Ni amount for improving the TE performance of β-$FeSi_2$ is smaller than 10% and 3%, respectively.

2. Experimental methods

The raw elements of iron (Fe grain 99.9% up), silicon (Si grain, 99.999%), cobalt (Co powder, 99% up), and nickel (Ni grain 99.9%) were prepared to follow the composition ratio of $Fe_{1-x}Co_xSi_2$ ($0 \le x \le 0.10$) and Ni-doped $Fe_{1-y}Ni_ySi_2$ ($0 \le y \le 0.03$). The raw materials were arc-melted under an argon atmosphere. Vacuum sealing was employed to remove the residual air before the heat treatment process. Two steps of heat treatment were applied. The first step is at 1423 K for 3 h and the second step is at 1113 K for 20 h. The first step of heat treatment is to further homogenize the material distribution and the second step is to transform the metallic phase (α-Fe_2Si_5 + ε-FeSi) to the semiconducting phase (β-$FeSi_2$). This heat treatment was followed in the previous report

* Corresponding author.
E-mail address: nakatsugawa-hiroshi-dx@ynu.ac.jp (H. Nakatsugawa).

https://doi.org/10.1016/j.ssc.2023.115287
Received 3 July 2023; Received in revised form 12 July 2023; Accepted 20 July 2023
Available online 21 July 2023

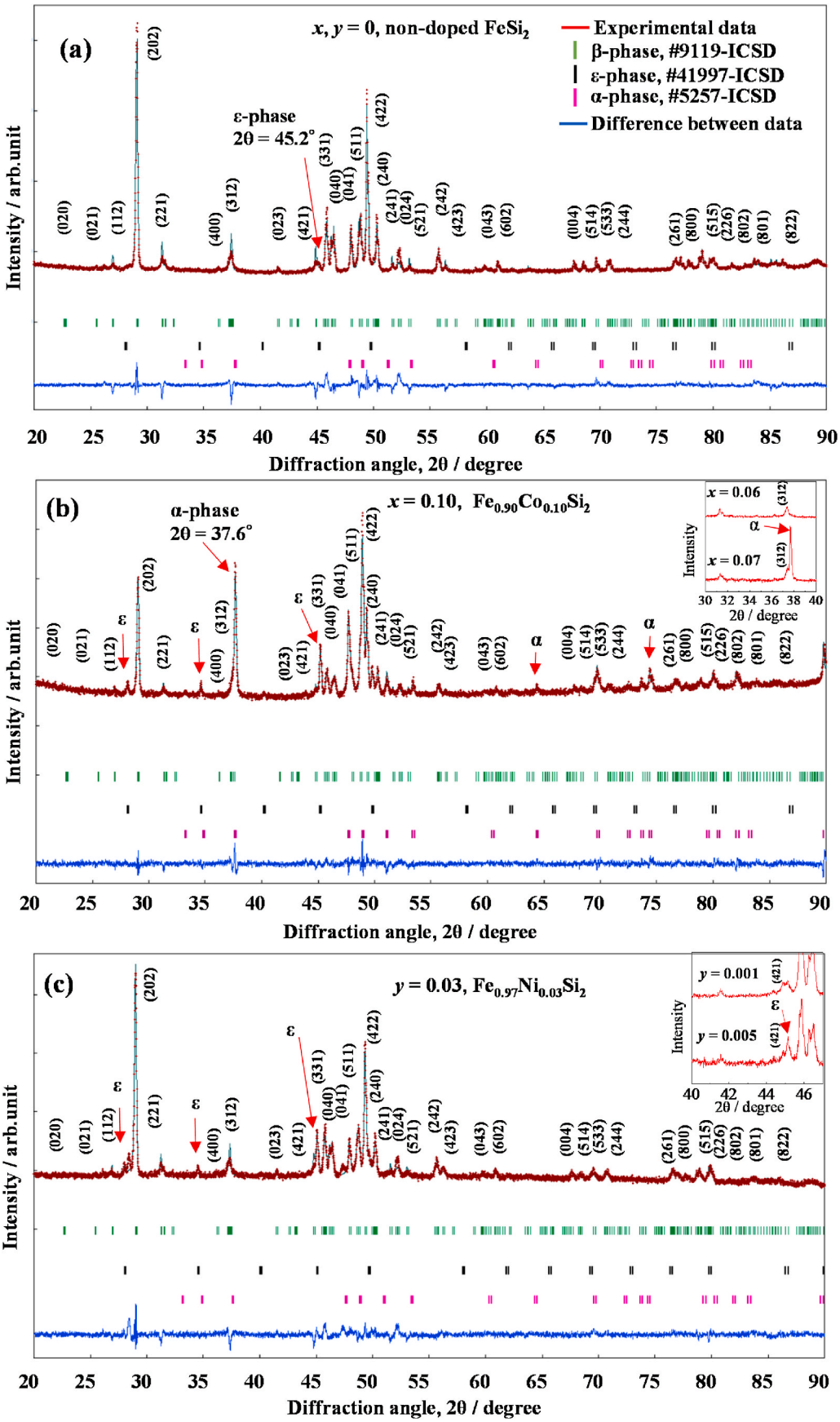

Fig. 1. Rietveld refinement of (a) non-doped $FeSi_2$, (b) $x = 0.10$, $Fe_{0.90}Co_{0.10}Si_2$, where the inset shows XRD patterns of $x = 0.06$ and $x = 0.07$, and (c) $y = 0.03$, $Fe_{0.97}Ni_{0.03}Si_2$, where the inset shows XRD patterns of $y = 0.001$ and $x = 0.005$. The indexed peaks are β-phase and arrows indicate the peak of metallic ε and α-phase.

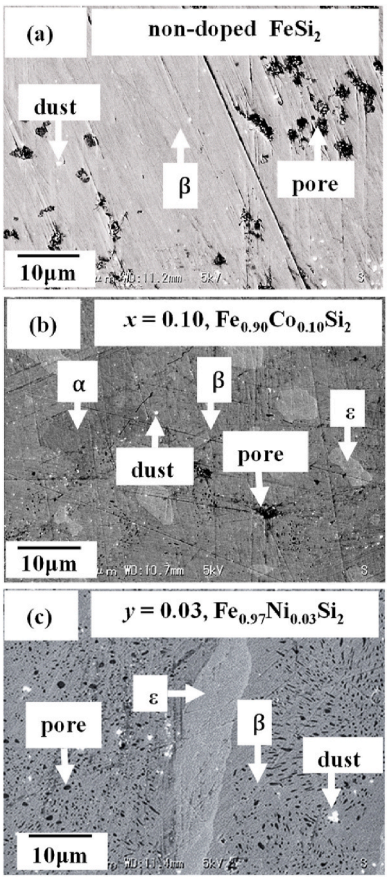

Fig. 2. SEM images of (a) non-doped $FeSi_2$ with only β-phase is observed, (b) $x = 0.10$, $Fe_{0.90}Co_{0.10}Si_2$ where the β, ε, and α-phases are observed, and (c) $y = 0.03$, $Fe_{0.97}Ni_{0.03}Si_2$ where the β and ε-phases are observed.

[4], where the optimum condition was identified.

The powder X-ray diffraction (XRD) patterns were measured by using an X-ray generator with Cu Kα radiation (High-resolution SmartLab, Rigaku). The measured XRD data were then used for the Rietveld analysis by utilizing the RIETAN-FP program. The crystal standard data were taken from Inorganic Crystal Structure Database (ICSD), where the code 9119-ICSD was used for β-phase [3], code 41997-ICSD was used for ε-phase [18], and code 5257-ICSD for α-phase [19]. In addition, the surface microstructure was observed by a 3D Real Surface View Microscope (VE8800, KEYENCE). The Seebeck coefficient (S) and electrical resistivity (ρ) were measured by using ResiTest8300 (TOYO Co.) and home-built apparatus. The thermal conductivity was measured by a power efficiency measurement system (PEM-2, ULVAC, Inc).

3. Results and discussion

The Rietveld refinement of the samples after the heat treatment process is plotted in Fig. 1. For non-doped $FeSi_2$, the majority of β-phase is obtained with a small peak of ε-phase at a diffraction angle of $2\theta = 45.2^\circ$ (in Fig. 1(a)). In Fig. 1(b), for Co doping, the peak of ε-phase at $2\theta = 45.2^\circ$ increases if we compare it to a non-doped sample. This pattern is similar to the previous report of Dabrowski et al. when 3% of Co is added to β-$FeSi_2$ [11]. In addition, the peak of α-phase also significantly increases at $2\theta = 37.6^\circ$ because of the high amount (10%) of dopant. The presence of α-phase agrees with the previous of Ito et al. when co-doping (Cu + Co) is introduced to β-$FeSi_2$ [13], indicating that the α-phase is formed when more impurities/dopants are added. On the other hand, in Fig. 1(c), the Ni addition only increases the peak of the ε-phase. This tendency is the same as the previous report for Ni-doped β-$FeSi_2$ prepared by mechanical milling and hot-pressing method reported by Nagai et al. [15].

Fig. 2 shows the microstructures visualized by SEM measurement. For non-doped $FeSi_2$, there is no presence of metallic phases, indicating almost a single β-phase is obtained (in Fig. 2(a)). This result agrees with the previous report of Dabrowski et al. [11]. Interestingly, for $Fe_{0.90}Co_{0.10}Si_2$, the grains of ε and α-phase are formed as can be seen in Fig. 2(b). This tendency is consistent with the Rietveld refinement in Fig. 1, where the peak of ε and α-phases increase with Co addition. Previous studies also reported that more metallic ε-phases were formed when B_4C [20], Cu [12], and rare-earth oxides [21] were introduced to β-$FeSi_2$. Fig. 2(c) shows that a large grain of ε-phase formed in the $Fe_{0.97}Ni_{0.03}Si_2$, but α-phase cannot be observed. This tendency suggests that the addition of Ni is more dominant to the formation of the ε-phase than the α-phase.

The phase fraction in the $Fe_{1-x}Co_xSi_2$ is plotted in Fig. 3 and the data are summarized in Table 1 The amount of β-phase decreases from 97.52% to 41.53% as x increases from 0 to 0.10, respectively. In contrast, the mass fraction of both ε and α-phase remarkably increases with x, indicating the phase transition is drastically influenced by the dopant. With increasing x from 0 to 0.10, the ε-phase increases from 1.41% to 9.36%, and the α-phase increases from 1.07% to 49.11%. This result suggests that the increase in α-phase is more dominant than the ε-phase for $Fe_{1-x}Co_xSi_2$. This is because the atomic size of Co ($r_{Co} = 1.26$ Å) is larger than Fe ($r_{Fe} = 1.25$ Å). Therefore, the orthorhombic structure of β-$FeSi_2$ transforms to the tetragonal structure of α-Fe_2Si_5, whereas the lattice constant, $a = 9.8868(2)$ Å, of orthorhombic β-phase is approximately twice larger than lattice constant, $c = 5.151(1)$ Å, of tetragonal α-phase. In addition, the decrease in solubility of Co in the β-phase with increasing x should also be the factor to increase the metallic α-phase. The amount of α-phase and β-phase is stable for $0.01 \leq x \leq 0.06$, and then α-phase suddenly increases for $x > 0.06$ but β-phase decreases. This result suggests that the maximum solid solution limit of Co in the β-phase is 6%. This tendency agrees with the previous report of Ware et al., where the maximum solubility of $CoSi_2$ in β-$FeSi_2$ is 6% [22]. In addition, it is consistent with the XRD patterns in the **inset of** Fig. 1 **(b)**, where the peak of α-phase at $2\theta = 37.6^\circ$ is dominant at $x = 0.07$. It is considered that the optimum Co doping amount to improve TE properties should be smaller than 6%.

Fig. 4 shows the mass fraction in the $Fe_{1-y}Ni_ySi_2$. With increasing y, the β-phase moderately decreases from 97.52% to 89.61% but the ε-phase increases from 1.41% to 9.28%. The change in α-phase is negligible. This tendency suggests that the increase in ε-phase is more dominant than α-phases for the $Fe_{1-y}Ni_ySi_2$. This is because the atomic size of Ni ($r_{Ni} = 1.21$ Å) is smaller than Fe ($r_{Fe} = 1.25$ Å). As a result, the orthorhombic structure of β-$FeSi_2$ transforms into the cubic structure of ε-FeSi, whereas lattice constants of cubic ε-phase, $a = b = c = 4.4858(5)$ Å, are smaller than lattice constant orthorhombic β-phase. In addition, the decrease in solubility of Ni in the β-phase with increasing its content should also be the factor to increase the metallic ε-phase. In the XRD patterns of the **inset of** Fig. 1 **(c)**, the peak of ε-phase at $2\theta = 45.2^\circ$ is dominant at $y = 0.005$. Therefore, it is considered that the maximum solubility of Ni in the β-phase is smaller than 0.5%.

The Seebeck coefficient (S), electrical resistivity (ρ), and thermal conductivity (κ) at room temperature of $Fe_{1-x}Co_xSi_2$ with Co dependence are plotted in the inset of Fig. 3. The absolute $|S|$ of the non-doped sample is smaller than the Co-doped samples probably due to the decrease in carrier mobility but the $|S|$ decreases with increasing x as shown in the inset (a) of Fig. 3. The ρ decreases with Co doping level x as shown in the inset (b) of Fig. 3. The decrease in both $|S|$ and ρ with increasing x is because of the increase in carrier concentration [23] and metallic phase. In the inset (c) of Fig. 3, the κ slightly decreases with x because of the electron and phonon interaction between the dopant and host atom as indicated by Tani et al. [24]. In addition, the S, ρ, and κ at 300 K of $Fe_{1-y}Ni_ySi_2$ with Ni dependence are plotted in the inset of Fig. 4. In the inset (a)–(b) of Fig. 4, both S and ρ remarkably decrease with y

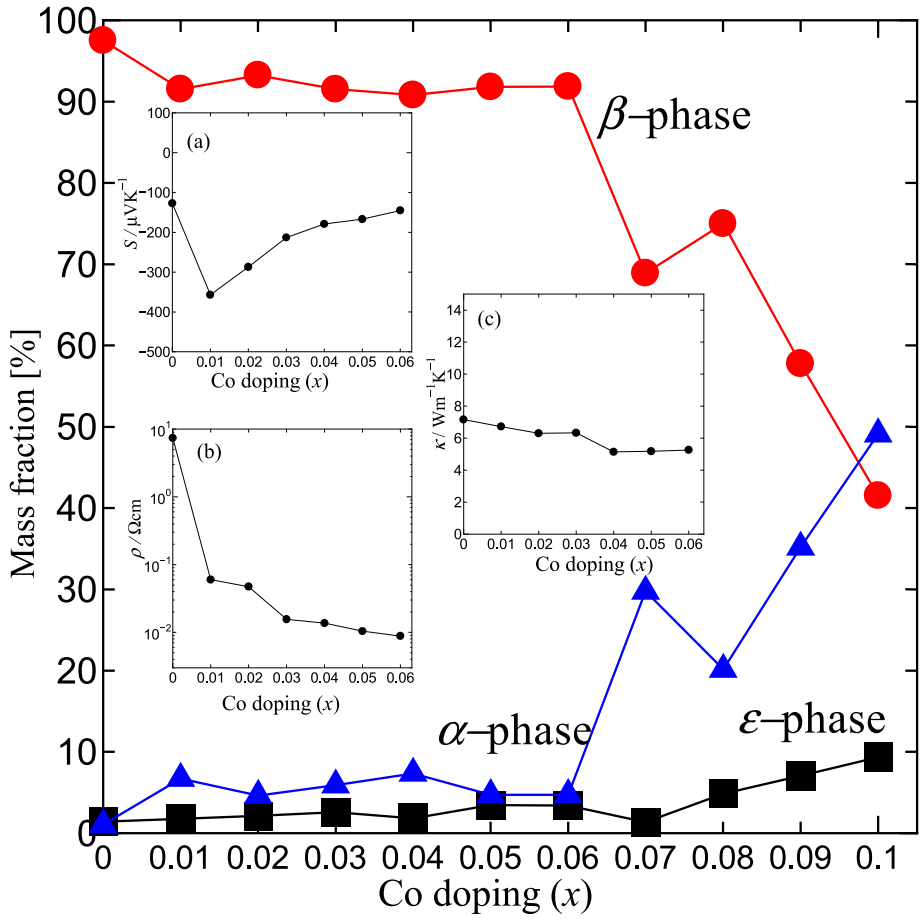

Fig. 3. Mass fraction of Co-doped $Fe_{1-x}Co_xSi_2$ with x dependence calculated by Rietveld analysis. The inset shows the data of (a) Seebeck coefficient, S, (b) electrical resistivity, ρ, and (c) thermal conductivity, κ, at room temperature.

Table 1
Mass fraction of β, ε, and α-phase in $Fe_{1-x}Co_xSi_2$ and $Fe_{1-y}Ni_ySi_2$.

x	Mass fraction in $Fe_{1-x}Co_xSi_2$		
	β-phase (%)	ε-phase (%)	α-phase (%)
0.00	97.52	1.41	1.07
0.01	91.53	1.76	6.72
0.02	93.24	2.13	4.63
0.03	91.52	2.57	5.91
0.04	90.81	1.83	7.35
0.05	91.81	3.46	4.73
0.06	91.86	3.41	4.73
0.07	68.89	1.34	29.76
0.08	75.00	4.84	20.15
0.09	57.77	7.06	35.17
0.10	41.53	9.36	49.11
y	Mass fraction in $Fe_{1-y}Ni_ySi_2$		
	β-phase (%)	ε-phase (%)	α-phase (%)
0.00	97.52	1.41	1.07
0.01	95.21	4.37	0.442
0.02	91.96	6.91	1.12
0.03	89.61	9.28	1.12

because of the increase in carrier density [23] and metallic phase. The variation of κ with Ni dependence is negligible as shown in the inset (c) of Fig. 4.

Fig. 5 shows the power factor (*PF*) of the $Fe_{1-x}Co_xSi_2$ and $Fe_{1-y}Ni_ySi_2$. The *PF* value is calculated by $PF = S^2\rho^{-1}$, where S is the Seebeck coefficient and ρ is the electrical resistivity of the material. When Co or Ni is added into the β-$FeSi_2$ system, both the Seebeck coefficient and electrical resistivity decrease due to the increase in n_H because Co and Ni act as the donner to β-$FeSi_2$. Importantly, the formation of metallic phases also contributes to the decrease in $|S|$ and ρ. Fig. 5(a) shows the maximum *PF* values of 291 $\mu Wm^{-1}K^{-2}$ at 300 K and 900 $\mu Wm^{-1}K^{-2}$ at 800 K obtained in the $x = 0.03$ sample. It is considered that $x = 0.03$ is the optimum doping concentration. When x is higher than 0.03, the *PF* value decreases due to the reduction in $|S|$. It is because the amount of β-phase decreases with increasing x (Table 1). In other words, more metallic phases are formed when more Co is added to the β-$FeSi_2$. This result supports phase fraction analysis, whereases the optimum doping concentration is between $0 \leq x \leq 0.06$ because β-phase remarkably decreases at $x > 0.06$. For the Co-doped sample, the maximum *PF* value of the current study (900 $\mu Wm^{-1}K^{-2}$ at 800 K) is higher than the sample prepared by pressure sintering (800 $\mu Wm^{-1}K^{-2}$ at 800 K) as reported by Shibuya et al. [25] and hot pressing method (500 $\mu Wm^{-1}K^{-2}$ at 600 K) as reported by Ito et al. [13] due to the higher $|S|$. It is probably because Shibuya et al. and Ito et al. applied a shorter heat treatment time of 5 min and 60 min, respectively. As a result, more metallic phases still remained in their samples, reducing $|S|$. In Fig. 5(b), for $Fe_{1-y}Ni_ySi_2$, the highest *PF* values of 13 $\mu Wm^{-1}K^{-2}$ at 300 K and 200 $\mu Wm^{-1}K^{-2}$ at 600 K are obtained in the $y = 0.001$ sample. When y is higher than 0.001, the *PF* values decrease due to the reduced amount of semiconducting β-phase as shown in Table 1. It should be noted that the decrease in $|S|$ is very sensitive to the presence of a metallic phase, resulting in a reduction in *PF* value. For the Ni-doped sample, at room temperature, the maximum *PF* value of the current study (13 $\mu Wm^{-1}K^{-2}$) is almost the same as the thin film sample (17 $\mu Wm^{-1}K^{-2}$) prepared RF sputtering method as reported by Komabayashi et al. [26]. However, at high temperatures, the maximum *PF* value of the current work (200

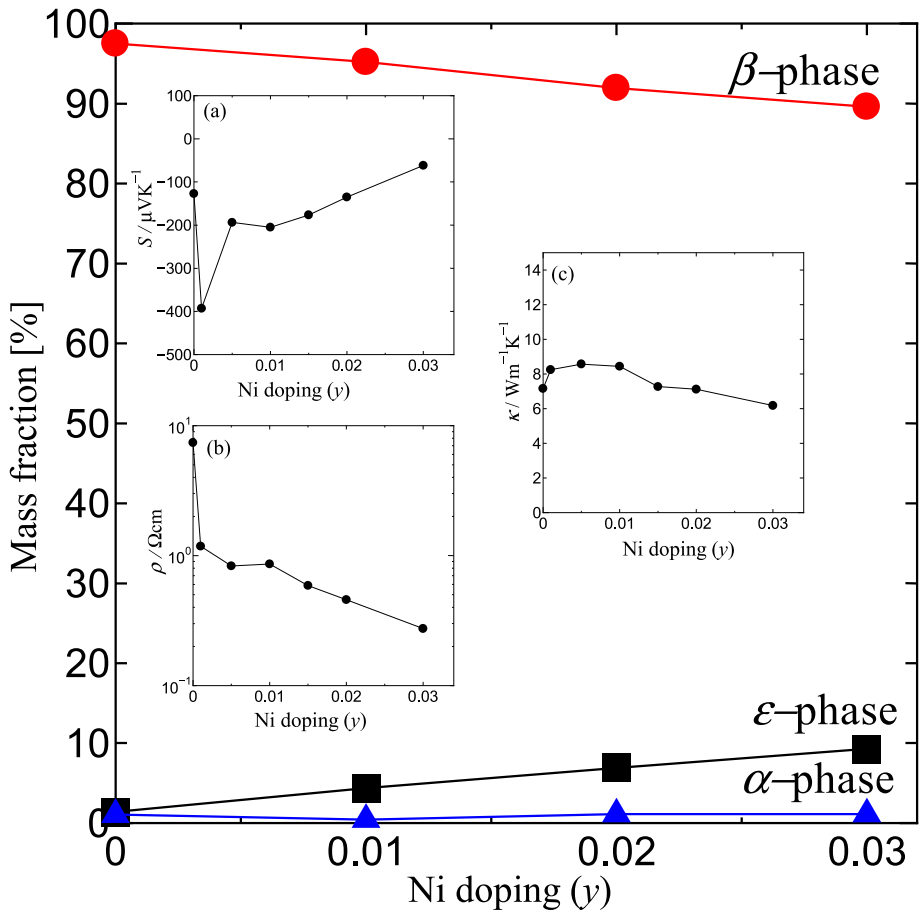

Fig. 4. Mass fraction of Ni-doped $Fe_{1-y}Ni_ySi_2$ with y dependence calculated by Rietveld analysis. The inset shows the data of (a) Seebeck coefficient, S, (b) electrical resistivity, ρ, and (c) thermal conductivity, κ, at room temperature.

$\mu Wm^{-1}K^{-2}$ at 600 K) is higher than the bulk sample of the previous report of Nagai et al. prepared by the hot-pressed method (50 $\mu Wm^{-1}K^{-2}$ at 650 K) [15] because the heat treatment was not applied to their samples, resulting in the remained large amount of metallic phase and consequently decrease $|S|$. At the same doping level, the *PF* value of the Ni-doped sample is lower than the Co-doped sample because the Ni has a lower solid solution limit than Co in the β-$FeSi_2$ [15,27]. Therefore, at the same doping level, the n_H of the Ni-doped sample is lower than the Co-doped sample [23]. Consequently, the ρ of the Co-doped sample is lower than the Ni-doped sample, making the *PF* value of the Co-doped sample higher than the Ni-doped samples. The *ZT* value calculated by $ZT = S^2\ T\rho^{-1}\kappa^{-1}$, where S is Seebeck coefficient, T is temperature, ρ is electrical resistivity, and κ is thermal conductivity, with Co and Ni dependence is plotted in Fig. 5. At 300 K, the *ZT* values of both Co and Ni-doped samples are higher than the non-doped sample, having a similar tendency to *PF* value. In Fig. 5(a), at 800 K, the highest *ZT* of 0.099 is obtained in 3% Co doping. In Fig. 5(b), at 600 K, the highest *ZT* of 0.019 is obtained in 0.1% Ni doping sample. It is considered that the variation of *ZT* values is mainly contributed by the *PF* values.

4. Conclusions

In summary, we have investigated the mass fraction of β-$Fe_{1-x}Co_xSi_2$ ($0 \le x \le 0.10$) and β-$Fe_{1-y}Ni_ySi_2$ ($0 \le y \le 0.03$) prepared by arc melting and heat treatment. In the β-$Fe_{1-x}Co_xSi_2$ system, the increase in α-phase is more dominant than ε-phase, where the amount of α-phase increases from 1.07 to 49.11% as x increases from 0 to 0.10. In contrast, in the β-$Fe_{1-y}Ni_ySi_2$ system, the increase in ε-phase is more dominant than α-phase, where the amount of ε-phase increases from 1.41% to 9.28% as y increases from 0 to 0.03. This study offers a solution to evaluate the phase fraction in Co and Ni-doped β-$FeSi_2$. Therefore, we could identify the range of optimum dopant concentration to prepare Co and Ni-doped β-$FeSi_2$ for thermoelectric application with a preferable phase.

Author statement

Conceptualization: S. Sam and H. Nakatsugawa, Investigation: S. Sam, H. Nakatsugawa, and K. Yamazaki, Formal analysis: S. Sam, H. Nakatsugawa, and K. Yamazaki, Writing original draft: S. Sam and H. Nakatsugawa.

Declaration of competing interest

The authors declare that they have no known competing financial interests or personal relationships that could have appeared to influence the work reported in this paper.

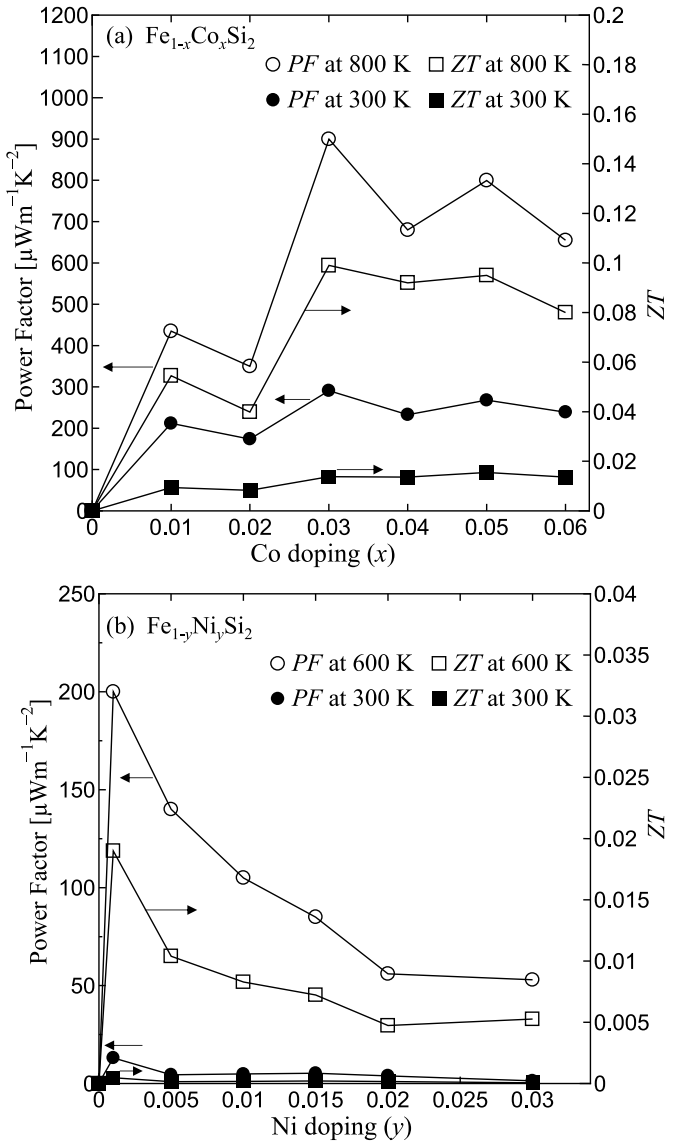

Fig. 5. Power factor (*PF*) and *ZT* values of (a) $Fe_{1-x}Co_xSi_2$ with *x* dependence and (b) $Fe_{1-y}Ni_ySi_2$ with *y* dependence. The left and right axis represent the *PF* and *ZT*, respectively. The solid circles and squares are the data at 300 K of *PF* and *ZT*, respectively. The open circles and squares in Fig. 5(a) show the data at 800 K of $Fe_{1-x}Co_xSi_2$ of *PF* and *ZT*, respectively, and Fig. 5(b) shows the data at 600 K of $Fe_{1-y}Ni_ySi_2$.

Data availability

The data that has been used is confidential.

Acknowledgements

This XRD and SEM measurement was carried out by using the equipment of Yokohama National University, Instrumental Analysis, and Evaluation Center. This work was partly supported by the Japanese government (MEXT) scholarship for the Department of mechanical engineering, materials science, and ocean engineering.

References

[1] T. Sakata, Y. Sakai, H. Yoshino, H. Fujii, I. Nishida, J. Less Common Met. 61 (1978) 301–308.
[2] L. Pauling, A.M. Soldate, Acta Crystallogr. 1 (1948) 212–216.
[3] Y. Dusausoy, J. Protas, R. Wandji, B. Roques, Acta Crystallogr. Sect. B Struct. Crystallogr. Cryst. Chem. 27 (1971) 1209–1218.
[4] M. Ohtaki, D. Ogura, K. Eguchi, H. Arai, Chem. Lett. 22 (1993) 1067–1070.
[5] Y. Isoda, H. Udono, Preparation and thermoelectric properties of iron disilicide, in: D.M. Rowe (Ed.), Thermoelectr. Its Energy Harvest, first ed., CRC Press, 2012, pp. 18–25, 1-18.
[6] A. Binti Abdullah Zaik, F. Liana Binti Mohd Redzuan, S. Ahmad Zaki Bin Shaikh Salim, A. Faiz Bin Mohammad, M. Fitri Bin Mohd Yakub, M. Takeda, Mater. Today Proc. 65 (2022) 2979–2985.
[7] J.J. Gong, A.J. Hong, J. Shuai, L. Li, Z.B. Yan, Z.F. Ren, J.-M. Liu, Phys. Chem. Chem. Phys. 18 (2016) 16566–16574.
[8] J. Tani, H. Kido, J. Appl. Phys. 86 (1999) 464–467.
[9] M. Ito, H. Nagai, E. Oda, S. Katsuyama, K. Majima, J. Appl. Phys. 91 (2002) 2138–2142.
[10] X. Du, P. Qiu, J. Chai, T. Mao, P. Hu, J. Yang, Y.-Y. Sun, X. Shi, L. Chen, ACS Appl. Mater. Interfaces 12 (2020) 12901–12909.
[11] F. Dąbrowski, Ł. Ciupiński, J. Zdunek, J. Kruszewski, R. Zybała, A. Michalski, K. Jan Kurzydłowski, Mater. Today Proc. 8 (2019) 531–539.
[12] M. Ito, H. Nagai, D. Harimoto, S. Katsuyama, K. Majima, J. Alloys Compd. 322 (2001) 226–232.
[13] M. Ito, H. Nagai, T. Tanaka, S. Katsuyama, K. Majima, J. Alloys Compd. 319 (2001) 303–311.
[14] S. Sam, H. Nakatsugawa, Y. Okamoto, Jpn. J. Appl. Phys. 61 (2022), 111002.
[15] H. Nagai, I. Maeda, S. Katsuyama, K. Majima, J. Jpn. Soc. Powder Powder Metall. 41 (1994) 560–564.
[16] S. Sam, S. Odagawa, H. Nakatsugawa, Y. Okamoto, Materials 16 (2023) 927.
[17] S. Sam, H. Nakatsugawa, Y. Okamoto, Mater. Adv. 4 (2023) 2821–2830.
[18] B.C. Sales, E.C. Jones, B.C. Chakoumakos, J.A. Fernandez-Baca, H.E. Harmon, J. W. Sharp, E.H. Volckmann, Phys. Rev. B 50 (1994) 8207–8213.
[19] G. Li, W. Bai, N. Shi, Q. Fang, M. Xiong, J. Yang, Z. Ma, H. Rong, Eur. J. Mineral 24 (2012) 1047–1052.
[20] F. Dąbrowski, Ciupiński, J. Zdunek, W. Chromiński, M. Kruszewski, R. Zybała, A. Michalski, K.J. Kurzydłowski, Arch. Metall. Mater. 66 (2021) 1157–1162.
[21] M. Ito, T. Tada, S. Katsuyama, J. Alloys Compd. 350 (2003) 296–302.
[22] R.M. Ware, D.J. McNeill, Proc. Inst. Electr. Eng. 111 (1964) 178–182.
[23] J. Tani, H. Kido, J. Appl. Phys. 84 (1998) 1408–1411.
[24] J. Tani, H. Kido, Jpn. J. Appl. Phys. 40 (2001) 3236.
[25] M. Shibuya, M. Kawata, Y. Shinohara, M. Ohyanagi, Trans. Mater. Res. Soc. Japan. 40 (2015) 219–222.
[26] M. Komabayashi, K.I. Hijikata, S. Ido, Jpn. J. Appl. Phys. 30 (1991) 331–334.
[27] T. Kojima, K. Masumoto, M. Okamoto, I. Nishida, J. Less Common Met. 159 (1990) 299–305.